Growth of single-crystal imine-linked covalent organic frameworks using amphiphilic amino-acid derivatives in water

Growth of single-crystal imine-linked covalent organic frameworks using amphiphilic amino-acid derivatives in water

Zhipeng Zhou[1,11], Lei Zhang[2,11], Yonghang Yang[1], Iñigo J. Vitorica-Yrezabal[3], Honglei Wang[1], Fanglin Tan[1], Li Gong[4], Yuyao Li[1], Pohua Chen[2], Xin Dong[1], Zihao Liang[1], Jing Yang[5], Chao Wang[6], Yuexian Hong[1], Yi Qiu[2], Armin Gölzhäuser[7], Xudong Chen[1,8,9], Haoyuan Qi[10], Sihai Yang[3], Wei Liu[5,9]✉, Junliang Sun[2]✉ & Zhikun Zheng[1,8,9]✉

[1]Key Laboratory for Polymeric Composite and Functional Materials of Ministry of Education, School of Chemistry, and State Key Laboratory of Optoelectronic Materials and Technologies, Sun Yat-sen University, Guangzhou, China.

[2]College of Chemistry and Molecular Engineering, Beijing National Laboratory for Molecular Sciences Peking University, Beijing, China.

[3] Department of Chemistry and Photon Science Institute, The University of Manchester, Manchester, UK.

[4]Instrumental Analysis Research Center, Sun Yat-sen University, Guangzhou, China.

[5]Key Laboratory of Low-Carbon Chemistry & Energy Conservation of Guangdong Province, Key Laboratory for Polymeric Composite and Functional Materials of Ministry of Education, School of Materials Science and Engineering, and State Key Laboratory of Optoelectronic Materials and Technologies, Sun Yat-sen University, Guangzhou, China.

[6]MOE Key Laboratory of Bioinorganic and Synthetic Chemistry, School of Chemistry, Sun Yat-Sen University, Guangzhou, China.

[7]Faculty of Physics, Bielefeld University, Bielefeld, Germany.

[8]School of Chemical Engineering and Light Industry, Guangdong University of Technology, Guangzhou 510006, P. R. China

[9] Jieyang Branch of Chemistry and Chemical Engineering Guangdong Laboratory, Jieyang, Guangdong 515200, China

[10]Central Facility of Electron Microscopy, Electron Microscopy Group of Materials Science, Universität Ulm, Ulm, Germany.

[11]These authors contributed equally to this work.

✉email: liuw226@mail.sysu.edu.cn; junliang.sun@pku.edu.cn; zhengzhikun@mail.sysu.edu.cn

Abstract: A core feature of covalent organic frameworks (COFs) is crystallinity, but current crystallization processes rely substantially on trial and error, chemical intuition and large-scale screening that typically require harsh conditions and low levels of supersaturation, hampering the controlled synthesis of single-crystal COFs, particularly on large scales. Here, we report a strategy to produce single-crystal imine-linked COFs in aqueous solutions under ambient conditions using amphiphilic amino-acid derivatives with long hydrophobic chains. We propose that these amphiphilic molecules self-assemble into micelles that serve as dynamic barriers to separate monomers in aqueous solution (nodes) and hydrophobic compartments of the micelles (linkers), thereby regulating the polymerization and crystallization processes. Disordered polyimines were obtained in the micelle, which were then converted into crystals in a step-by-step fashion. Five different three-dimensional COFs and a two-dimensional COF were obtained as single crystals on the gram-scale, with yields of 92% and above.

Introduction

Covalent organic frameworks (COFs), constructed from organic monomers termed as nodes and linkers through covalent bonds, are crystalline polymers with permanent porosity[1,2]. Their synthesis typically involves volatile organic solvents, high temperature, high pressure and inert atmosphere or vacuum[3,4]. During the synthesis, amorphous polymeric materials forms spontaneously, aggregates and precipitates rapidly, and depends on random error-corrections offered by microscopic reversibility of the dynamic covalent bonds to crystallize into network structures[5]. The free polymerization and crystallization process naturally requires trial and error, chemical intuition and large-scale screening to find an experimental condition to crystallize a specific structure[6], and prevents the formation of single crystal COFs with controlled size and their large-scale synthesis[7,8]. A simple, general, and scalable strategy thus remains to be developed to produce single-crystal COFs.

In this article, we proposed to use micelles of amphiphilic amino-acid derivatives with long hydrophobic chains to prevent the precipitation of materials from polymerization of the monomers through weak interactions (hydrogen bond, electrostatic interactions and hydrophobic-hydrophobic interactions)[9-11] in water to synthesize single-crystal COFs (Fig. 1). Imine-linked ones were selected due to the high reversibility of the linkage in water as well as their high chemical stability for COFs[4]. We monitored the polymerization and crystallization process, investigated the basic building units for the crystal growth, studied the crystallization mechanism and proposed the crystal growth model. To understand the effects of different parameters on the crystallization, the length of the hydrophobic chain of the amphiphilic molecules of amino-acid derivatives, their head groups, added catalysts, reaction temperature and cationic ions which can coordinate with the amino-acid derivatives were investigated. To show the generality of the synthesis strategy, we produced five types of three-dimensional and one two-dimensional single-crystalline COFs at the gram-scale with yields of ≥ 92%. A two-dimensional COF-366 was also synthesized at the air–water interface.

Results and Discussion

Crystallization strategy and process. For the crystallization of COFs, C_{16}-GlyA was synthesized from palmitoyl chloride and glycine (Supplementary Information Section 1.1). It can assemble into micelles with a layered supramolecular structure of around 331 nm in water (Extended Data Fig. 1a, b and Supplementary

Fig. 2 and Supplementary Table 1), affording a hydrophobic compartment[12]. We started with COF-301 that was in previous work only obtained as poorly crystalline aggregates with a low yield and no structure elucidation could be enabled despite of its high promise in different areas[13, 14] by condensation of 2,5-dihydroxy-1,4-benzenedicarboxaldehyde (linker **A**) with one equivalent of tetrakis(4-aminophenyl)methane (TAM) under ambient conditions. Solution nuclear magnetic resonance (NMR) and electrospray ionization high-resolution mass spectrometry indicated that TAM protonated with *p*-toluenesulfonic acid (PTSA) mainly dissolved in water while linker **A** was in the C_{16}-GlyA phase when added individually (Extended Data Fig. 1a, b and Extended Data Fig. 2). When powders of linker **A** were added into the C_{16}-GlyA emulsion, it tuned from white to yellow. The size of the micelles grew to ~ 503 nm and no precipitate or micelles of other size was detected (Extended Data Fig. 1a), furthering confirming the dissolution of the monomer in the C_{16}-GlyA phase. Subsequent addition of PTSA-protonated TAM led to gel-like mixtures within 10 minutes. After thorough rinsing with water and tetrahydrofuran, disordered solid phase with a yield of 91% was obtained (Fig. 1d and Extended Data Fig. 3a, b, c, d). No monomers were detected in the solid phase by high-resolution mass spectrometry, and the broad differential thermal gravity (DTG) peak suggested existence of a mixture of materials (Fig. 2a), and Fourier transform infrared (FTIR) spectra indicated they were polyimines containing large amounts of free aldehyde groups (Extended Data Fig. 3e). The formation of the gel-like mixtures indicated the micelles have strong interactions with the polyimines most probably by hydrogen bonds, electrostatic interactions and hydrophobic-hydrophobic interactions.

We then evaluated the yield and crystallinity of the isolated solid phase at different reaction time. The yield showed no obvious time dependence and fluctuated between 91% and 95% (Fig. 2b). Bragg peaks of (2 0 0), (2 1 1) and (1 1 4) of COF-301 emerged after two days and single-crystal COF-301 could be clearly observed by optical microscopy (Extended Data Fig. 3c and Fig. 2c), suggesting a gradual amorphous-to-crystalline transition. As the reaction proceeded, the intensities of Bragg peaks increased, demonstrating gradual transformation of the disordered phase to crystals (Fig. 2b and Extended Data Fig. 3c, d). As also visualized by optical microscopy (Fig. 2c), 2 μm-sized crystals occurred on day two and more appeared with the increase of time. Pure single-crystal COF-301 was obtained after 14 days (Fig. 1e). They are uniform cuboids with typical length and width of around 2 μm and 0.6 μm (length/width = 3.3) at a molar concentration of linker **A** of 0.05 mol L^{-1}, respectively. Monodispersed single-crystals were obtained despite

the variation of the concentration of the monomers (nodes and linkers) by five orders of magnitude from 0.005 mmol L^{-1} to 0.5 mol L^{-1}, while poly-crystals, aggregated crystals or amorphous precipitate were typically obtained beyond low levels of supersaturation[5,6]. Notably, the size of the crystal increased from ~ 0.6 μm × 0.08 μm at 0.005 mmol L^{-1} to ~ 20 μm × 10 μm at 0.5 mol L^{-1} (Fig. 1f, g). The increase of the crystal size with the increase of the concentrations of the reactants in solution is contrary to the correlation in growth of polymer crystals from a saturated solution, a melt or a solid[15]. Meanwhile, in previous reports, practices such as the use of poor solvent to decrease the solubility of reactants, addition of reaction inhibitors/competitors and slow addition of reactants were employed to keep low concentrations of reactants to decrease amorphous parts and increase crystal size of COFs in contemporary methods [6-8].

Transmission electron microscopy (TEM) showed that there was ~ 30 nm of adsorbed layer on the surface of the crystals (Fig. 2d, left), which could be removed by rinsing with tetrahydrofuran (Fig. 2d, right). Characteristic peaks of C_{16}-GlyA in confocal Raman spectroscopy disappeared after rinsing, indicating the main component of the adsorbed layer was the amino-acid derivative (Extended Data Fig. 3f). Note that the weak interactions (mainly hydrophobic-hydrophobic and hydrogen bonding interactions) among C_{16}-GlyA were highly dynamic, which facilitated the diffusion of TAM and PTSA. We propose that deprotonated TAMs entered the hydrophobic phase of the micelles and reacted with linker **A**, trigging the nucleation and growth of the crystal, while PTSA-protonated TAMs diffused to water due to solubility (Extended Data Figs. 1 and 2).

Structural characterization. We selected an as-synthesized COF-301 (termed as COF-301-S) to prove single crystallinity and resolve the atomic structure with single-crystal XRD (Supplementary Fig. 3 and Supplementary Table 2). COF-301-S was single crystal with a tetragonal space group of $I4_1/a$ (a = 26.434(4) Å, c = 7.5876(15) Å) and 7-fold interpenetration. The single network exhibits a diamond-type topology in which each TAM molecule is connected to four linkers **A** (Fig. 3a). The refined data resolution was ~ 0.9 Å, and all non-hydrogen atoms in the COF-301-S were identified. The selected area electron diffraction showed that the interpenetration direction, *i.e.* along the longest diagonal of the unit cage (Fig. 2c and Fig. 3a, black arrow indicates the direction), was parallel to the elongation direction of the cuboids. The COF-301-S has one-dimensional (1D) straight channels along the interpenetration direction. A notable framework distortion

was observed upon removal of C_{16}-GlyA by rinsing with tetrahydrofuran (Fig. 3b). The topology and interpenetration degree remained, while the pore size changed from 9.6 Å to 3.1 Å. The washed COF-301 (termed as COF-301-W) exhibited a different phase with a symmetry of $I2/c$ (a = 20.276(8) Å, b = 8.7098(18) Å, c = 20.212(4) Å, β = 99. 308(12) °) (Supplementary Fig. 9 and Supplementary Table 6).

Crystal growth model. We then investigated the surface morphology evolution of COF-301 to gain an insight into the crystal growth model. Aggregated crystals were prepared by dip coating aqueous solution of concentrated CCOF-301 on newly cleaved mica followed by blown dry in air for characterization with atomic force microscopy (AFM). Disparate surface morphologies on the top and side facets of the cuboids have been observed (Fig. 2e, f). The (010) plane exhibits a higher density of growth sites or kinks than (100)/(001) planes (Fig. 2c, e and f), which is a characteristic of adhesive growth in which the building units stochastically integrate into the growing surface[16]. The (100)/(001) planes, on the other hand, show a train of terraces indicating layer-by-layer growth in which the building units preferentially integrate into the kink sites along the terrace edge (Fig. 2f). Due to the limited number of kink sites, the growth rate of the layer-by-layer mode is lower than that of the adhesive mode[17, 18], leading to growth anisotropy. The line scans in Fig. 2e present the typical step sizes on the top surface, in which 0.22 nm, *i.e.* the height difference between interpenetrated networks, and its multiples have been identified (Fig. 2g). The terrace height on the (100)/(001) facets has four typical values (Fig. 2f), *i.e.* 1.0 nm (one TAM + one linker **A**), 1.3 nm (one TAM + two linkers **A**), 1.7 nm (two TAM + one linker-A), and 2.0 nm (two TAM + two linkers **A**) (Fig. 2h). The sub-unit-cell step heights on both the top and side facets suggest that monomers (nodes and linkers) and units consisting of a node and a linker are the main fundamental building units during the crystal growth. It indicates that the initially formed disordered polyimines acts as substrates for step-by-step growth of the crystals. This crystal growth pathway differs from the one found in contemporary synthesis methods for COFs and two-dimensional (2D) polymers[5, 19, 20], during which simultaneous polymerization and crystallization occurred followed by random error corrections directly on the reaction products.

Effects of experimental parameters. To understand the effects of different parameters on the isolated yield of the solid phase and its conversion ratio to single-crystal COFs, the length of the hydrophobic chain of the amphiphilic molecules of amino-acid derivatives and their head groups and added catalysts were investigated.

We first performed control experiments without C_{16}-GlyA, no solid was obtained even over a month. We then synthesized octanoylglycine (C_8-GlyA), decanoylglycine (C_{10}-GlyA), dodecanoylglycine (C_{12}-GlyA), tetradecanoylglycine (C_{14}-GlyA) and stearoylglycine (C_{18}-GlyA) (Supplementary Information Section 1.1) to investigate the effects of the length of the hydrophobic chain of the glycine derivatives (Extended Data Fig. 4a). Little solid was obtained for C_8-GlyA, C_{10}-GlyA, and C_{12}-GlyA, the yield of solid phase and crystals was 87% and 79% for C_{14}-GlyA, and then both reached maximum for C_{16}-GlyA. With C_{18}-GlyA, the yield of solid phase decreased to 79% (Extended Data Fig. 4a). The results indicated that the hydrophobicity and order of the assembled structure of the derivatives played important roles in regulating the diffusion, polymerization and crystallization process for the formation of COF-301. C_8-GlyA, C_{10}-GlyA, and C_{12}-GlyA were packed too loosely to form micelles, and therefore unable to regulate these processes[21]. With the increase of the chain length, and therefore the enhancement of the hydrophobicity and order of the assembled structures, larger micelles were formed and higher yields were achieved (Extended Data Fig. 1a). The hydrophobicity of C_{18}-GlyA hindered its efficiency to be dispersed in water and therefore resulted in a low yield for the formation of COF-301. We also used palmitic acid ($CH_3(CH_2)_{14}COOH$) for the synthesis. It led to clusters with a yield of 81% (Extended Data Fig. 4b), indicating the glycine group played a crucial role in keeping COF-301 in well-defined shapes and as mono-dispersed particles. We further synthesized palmitoyl-*L*-alanine (C_{16}-*L*-AlaA), palmitoyl-*L*-phenylalanine (C_{16}-*L*-PhalaA), palmitoyl-*L*-valine (C_{16}-*L*-ValA) and (S)-3,3-dimethyl-2-palmitamidobutanoic acid (C_{16}-*L*-*t*LeuA) (Supplementary Information Section 1.1) to investigate the effects of steric hindrance near the polar groups of the amino-acid derivatives on the morphology, size and yield, and no significant difference was observed (Extended Data Fig. 4c).

Control experiment without adding PTSA led to disordered materials with a yield of 5% (Extended Data Fig. 5). The yield of single-crystal COF-301 increased with the increase of molar concentration of PTSA, reached maximum at six equivalent molar amounts to linker **A**, and slightly fluctuated thereafter. Meanwhile, the time needed for achieving pure crystals decreased and shortened to 3 days at 9 and 10 molar equivalents of PTSA (Extended Data Fig. 5). Acetic acid and hydrogen chloride were also utilized as catalysts, and they provided lower yield (Extended Data Fig. 6a). Hydrogen chloride could offer larger crystals than that with PTSA. This can be attributed to the stronger acidity of hydrogen chloride, which facilitates the hydrolysis of the disordered polyimines into nodes, linkers and node–linker moieties as building units for subsequent crystal

196 growth. The effect of temperature (25 °C and 75 °C) was also investigated. The size of the single crystals
197 increased with the decrease of temperature (Extended Data Fig. 6b, c). Furthermore, lithium hydroxide and
198 potassium hydroxide instead of sodium hydroxide were utilized to study the effect of cationic ions which can
199 coordinate with the derivatives of amino acid (Extended Data Fig. 1b), crystals with similar morphology and
200 sizes were obtained (Extended Data Fig. 6d, e).

201 **Generality of the developed strategy**. This synthesis strategy shows general applicability. We chose
202 monomers with parent core (terephthalaldehyde (linker **B**)), electron-accepting (2,3,5,6-
203 tetrafluoroterephthalaldehyde (linker **C**)), heterocyclic (pyridine-2,5-dicarbaldehyde (linker **D**)) besides the
204 electron-donating (linker-A) substitutions near aldehyde groups and monomers with different length (4,4'-
205 biphenyldicarboxaldehyde, linker **E**) to gain single-crystal COF-300, SYSU-8, SYSU-9 and COF-320 under
206 the same crystallization condition as the synthesis of COF-301 (Methods). Single-crystalline mono-dispersed
207 COFs were obtained in all cases (Fig. 1h, i and Extended Data Fig. 7a, b), though the substitutions can notably
208 affect the reaction activity of aldehyde groups and the crystallization process[7]. This is in sharp contrast to the
209 contemporary synthesis methods for COFs, such as the solvothermal method, which requires extensive
210 refinement of optimal reaction conditions on minor change in the monomer structure[6] (Supplementary
211 Information Fig. 1). All non-hydrogen atoms of the crystals were identified (Fig. 3c-3f and Supplementary
212 Information Section 2, 3). The typical size of as-synthesized SYSU-9 (termed as SYSU-9-S) was ~ 20 μm ×
213 3 μm (Fig. 1h), and its structure was determined by single-crystal XRD with a resolution of 1.1 Å (Fig.3e).
214 SYSU-9-S crystallized in the space group $I4_1$ (a = 26.461(4) Å, c = 7.4600(15) Å). The size of SYSU-8 was
215 ~ 15 μm × 3 μm (Fig. 1i). COF-320 crystallized in the space group $I4_1/a$ (a = 23.360(3) Å, c = 8.4300(17) Å)
216 and an interpenetration degree of 9-fold (Fig. 3c). The crystal phase was different from that synthesized by
217 solvothermal method and had higher symmetry[22], and allowed atomic structure by continuous rotation
218 electron diffraction with an increased resolution of ~ 0.9 Å (Supplementary Table 4 and 5). The size of COF-
219 300 could be down to 600 nm (Supplementary Information Section 1.3) which made it processable as colloids,
220 for example, into flexible films (Extended Data Fig. 8). All the synthesized COFs have one-dimensional (1D)
221 straight channels in which the substitutions distributed spirally, offering varied channel surfaces with
222 different polarity and pore size (COF-301-W: 3.1 Å; COF-300: 5.5 Å; SYSU-8: 5.0 Å; SYSU-9-W: 6.8 Å,
223 COF-320: 6.7 Å) (Fig. 3b-f). We then chose 2DCOF-TTA-TBA as an illustrative example to extend the

synthesis methodology to synthesize organic 2D materials due to their great potential to go beyond inorganic analogues such as graphene and MoS_2 and great potential as key materials for next-generation technologies[23]. AA stacked nanosheets with the space group *P-6* (a = 17.875 (8) Å, c = 3.4652 (11) Å) were obtained (Extended Data Fig. 7c and Supplementary Information Section 3). Its thickness was about 50 nm, and could be easily dispersed well in solvents such as water and filtered into thin films (Extended Data Fig. 8). Importantly, the sheets could also be exfoliated by sonication into nanosheets with a thickness down to around 0.7 nm, which corresponded to around 2 layers (Extended Data Fig. 8e). The formation of the imine bonds in all the crystals were also confirmed by solid-state ^{13}C cross-polarization magic angle spinning NMR, FTIR spectroscopy and thermogravimetric analysis (TGA), and permanent porosity of the COFs was confirmed by gas adsorption (Supplementary Information Section 4-7). By comparing the 77 K nitrogen adsorption of known COFs, COF-300 and COF-TTA-BTA, the strategy offered materials (COF-300: 1320 $cm^2\ g^{-1}$; COF-TTA-BTA: 1438 $cm^2\ g^{-1}$) with Brunauer-Emmett-Teller surface area slightly higher than best reported results from COFs obtained with contemporary methods.[24, 25] (Extended Data Fig. 9).

The C_{16}-*L*-*t*LeuA could also be spread on the water surface to induce the crystallization of COF-366 (Methods), a typical 2D COF [26]. Initially, amorphous films were formed and stabilized underneath C_{16}-*L*-*t*LeuA (Extended Data Fig. 9), and gradually transformed into crystalline film with micrometer-sized single-crystal domains. The high crystallinity of the domain enabled near-atomic structure observation by aberration-corrected high-resolution TEM with a resolution down to ~ 2 Å (Extended Data Fig. 10).

We further investigated the role of the pore structure and pore wall structure in tuning the porosity of the single-crystal COFs with adsorption of CO_2 at 195 K and 273 K (Fig. 4a, 4b). In the uptake of CO_2, 'gate type' sorption profile occurred at 195 K[27], and disappeared at 273 K. The gate opening pressure at which an abrupt increase in adsorption after a threshold pressure and the uptake of CO_2 could be tuned by varying the pore surface or adsorption temperature, allowing systematic controlling of the uptake. Among them, COF-300 offered a CO_2 uptake of 480 and 8.5 $cm^3\ g^{-1}$ (P/P_0 = 0.95) at 195 K and 273 K, respectively (Fig. 4a, b). The substitutions applied to COF-300 (P/P_0 = 0.95) significantly decreased the uptake at 195K, while increased by 294%, 384%, 624%, and 729% with COF-320 (25 $cm^3\ g^{-1}$), SYSU-8 (30 $cm^3\ g^{-1}$), COF-301 (53 $cm^3\ g^{-1}$), and SYSU-9 (62 $cm^3\ g^{-1}$) at 273 K, respectively.

Scaled-up production. A key obstacle in exploring the application of single-crystal COFs is mass production, which remains challenging to be resolved[28]. We demonstrated the capability of scale-up of the strategy with gram-scale production of single crystals of COF-301 (yield = 92%), COF-300 (yield = 95%), SYSU-8 (yield = 94%), SYSU-9 (yield = 93%), COF-320 (yield = 94%) and 2DCOF-TTA-BTA (yield = 92%) (Fig. 4c). In contrast, the yield of single-crystal COF-300 has been reported, which amounted to 49.8% [7]. Importantly, the amino-acid derivatives could be recovered by recrystallization with a recovering rate of ≥ 92%.

Conclusion

In summary, we developed a strategy for the facile production of single-crystal imine-linked COFs using amphiphilic amino-acid derivatives with hydrophobic alkyl chain of 14 to 18 carbons. The amphiphilic molecules formed micrometer-sized micelles and offered numerous hydrophobic compartments in aqueous solution, which allowed separation of amine- and aldehyde-monomers in different phases during their polymerization as well as crystallization process and prevent the formed polymeric materials from precipitation through weak interactions. We propose that the diffusion of amine-monomers across the interface of the two phases may be regulated by protonation/deprotonation due to solubility difference, thereby regulating the polymerization and crystallization process. The amine- and aldehyde-linked monomers first polymerized into disordered polyimines in the micelle solution regardless of concentration, then transformed into crystals in a step-by-step fashion with nodes, linkers, and node–linker moieties as main building units as indicated by AFM. With the strategy, gram-scale production of single crystals of COF-301, COF-300, SYSU-8, SYSU-9, COF-320 and COF-TTA-BTA were obtained in good yields; a two-dimensional COF-366 was also synthesized at the air–water interface.

Acknowledgements We thank financial support from National Natural Science Foundation of China (52061135103, 52173296, 21871009 and 22125102). The funders had no role in study design, data collection and analysis, decision to publish or preparation of the manuscript. Structure characterizations were supported by Instrumental Analysis and Research Center of Sun Yat-sen University and Institute of Chemistry, Chinese Academy of Sciences, Diamond Light Source (Didcot, UK). We thank Y. N. Fan for access to powder XRD and FT-IR, S. Y. Guan for access to NMR, X. H. Zhu for access to ESI-HRMS, and J. Li and S. A. Sapchenko for help with data collection of some materials.

Author contributions ZK. Z. initiated the project. ZK. Z. and W. L. coordinated the research. ZK. Z. and ZP. Z. designed the experiments. ZP. Z. performed most of the experimental work. L. Z., P. C. and J. S. performed cRED, and atomic structure analysis. Y. Y., Y. L. and F. T. helped with the synthesis. H. W., Y. Q. and X. D. carried out TEM and SAED. L. G. and Z. L. conducted AFM. I. Y. and S. Y. conducted synchrotron radiation single-crystal XRD. Y. H. and X. D. helped with the PXRD analysis. P. C. carried out the high resolution PXRD measurements. J. Y. and C. W. measured N_2 and CO_2 adsorption-desorption experiments. ZK. Z., ZP. Z., J. S., L. Z., W. L, and H. Q wrote the manuscript. All authors contributed to the proofreading of the manuscript.

Competing interests: The authors declare no competing interests.

Figure Legends

Fig. 1 | Synthesis protocol and morphology of COFs. a, Schematic view of the current strategy, which utilizes palmitoylglycine to create a hydrophobic compartment, through assembly of micelles, in which single-crystal COFs grow. **b**, Structures of the amphiphilic amino acid derivatives studied in this work. , **c**, Chemical structure of tetrakis(4-aminophenyl)methane (TAM), 5,10,15,20-Tetrakis (4-aminophenyl)-21H,23H-porphyrin (TAPP), monomer 4,4',4''-(1,3,5-triazine-2,4,6-triyl)trianiline (TTA), monomer benzene-1,3,5-tricarbaldehyde (BTA), as well as linkers **A** to **E**. **d-i**, Optical microscopy and scanning electron microscope (SEM) images of the synthesized products using C_{16}-GlyA in water under ambient conditions (COF-301: TAM and linker **A**; SYSU-8: TAM and linker **C**; SYSU-9: TAM and linker **D**).

Fig. 2 | Growth mechanism of single-crystal COF-301. a, Derivative Thermogravimetry (DTG) of solid precursors and COF-301. **b**, The evolution of the percentage of the yield and crystallinity of reaction products over time. **c**, The product at day two contained both amorphous materials and COF-301. **d**, Transmission electron microscopy images show the morphology of the crystals in the reaction system (left) before and (right) after cleaning with tetrahydrofuran. **e**, **f**, Atomic force microscopy (AFM) topographic images of the growing (0 1 0) (**e**) and (1 0 0)/ (0 0 1) facets (**f**) after being rinsed with tetrahydrofuran and dried in air. **g**, **h**, The structure viewed along the ***a*** axis (**g**) and ***b*** axis (**h**) direction of the COF-301-W.

Fig. 3 | Single-crystal structure of COFs. a, Single-fold diamond (*dia*) network and the 7-fold interpenetrated *dia* topology of COF-301-S. **b**, Structures of COF-301-S and COF-301-W. **c**, Single-fold diamond (*dia*) network and the 9-fold interpenetrated *dia* topology of COF-320. **d**, **e**, The structures of COF-300 (**d**), and SYSU-8 (**e**). **f**, Structure of SYSU-9 (termed as SYSU-9-S) before and after washing (termed as SYSU-9-W) with tetrahydrofuran. The brown/grey areas are accessible surface area (Connolly surface) determined by using a probe with the radius of 1.0 Å. Atoms of carbon are shown in grey, nitrogen in blue, oxygen in red, and fluorine in green. Disordered guest molecules within the pores are omitted for clarity.

Fig. 4 | CO_2 adsorption and scale-up production of single-crystal COFs. a,b, The adsorption properties of the COFs could be tuned significantly by varying their pore wall structures as indicated by CO_2 adsorption isotherm of COF-300, COF-301, SYSU-8/9 and COF-320 at 95 K (a) and 273 K (b). **c**, Photographic demonstration of gram-scale synthesis.

References:

1. Diercks, C. S. & Yaghi, O. M. The atom, the molecule, and the covalent organic framework. *Science* **355**, eaal1585 (2017).
2. Côté, A. P. et al. Porous, Crystalline, Covalent Organic Frameworks. *Science* **310**, 1166-1170 (2005).
3. Peng, L., Guo, Q., Song, C. et al. Ultra-fast single-crystal polymerization of large-sized covalent organic frameworks. *Nat. Commun.* **12**, 5077 (2021).
4. Geng, K. Y. et al. Covalent organic frameworks: Design, synthesis, and functions. *Chem. Rev.* **120**, 16, 8814–8933 (2020).
5. Smith, B. J. Overholts, Hwang, A. C. N. & Dichtel, W. R. Insight into the crystallization of amorphous imine-linked polymer networks to 2D covalent organic frameworks. *Chem. Commun.* **52**, 3690-3693 (2016).
6. Smith, B. J. & Dichtel, W. R. Mechanistic studies of 2D covalent organic frameworks rapidly polymerized from initially homogenous conditions. *J. Am. Chem. Soc.* **136**, 8783-8789 (2014).
7. Ma, T. Q. et al. Single-crystal x-ray diffraction structures of covalent organic frameworks. *Science* **361**, 48–52 (2018).
8. Evans, A. M. et al. Seeded growth of single-crystal two-dimensional covalent organic frameworks. *Science* **361**, 52–57 (2018).
9. Lowenstam, H. A. Minerals formed by organisms. *Science* **211,** 1126–1130 (1981).
10. Gower, L. B. et al. Biomimetic model systems for investigating the amorphous precursor pathway and its role in biomineralization. *Chem. Rev.* **108**, 4551–4627 (2008).
11. Pal, A., Ghosh, Y. K. & Bhattacharya S. Molecular mechanism of physical gelation of hydrocarbons by fatty acid amides of natural amino acids. *Tetrahedron* **63**, 7334-7348 (2007).
12. Sakai, N. & Matile, S. Conjugated polyimine dynamers as phase-sensitive membrane probes. *J. Am. Chem. Soc.* **140**, 11438−11443 (2018).

13. Li, Z. et al. Structural and Dimensional transformations between covalent organic frameworks via linker exchange. *Macromolecules* **52**, 1257−1265 (2019).

14. Pramudya, Y. & Mendoza-Cortes, J. L. Design principles for high H_2 storage using chelation of abundant transition metals in covalent organic frameworks for 0-700 bar at 298K. *J. Am. Chem. Soc.* **138**, 15204−15213 (2016).

15. Pritula, I. & Sangwal, K. *Fundamentals of Crystal Growth from Solutions. Handbook of Crystal Growth: Bulk Crystal Growth Ed. P. Rudolph, 2nd ed.* (Elsevier, 2015, pp. 1185–1227).

16. Markov, I. V. *Crystal Growth and Epitaxy, Crystal Growth for Beginners: Fundamentals of Nucleation* (World Scientific, Singapore, 2016).

17. Lovette, M. A. et al. Crystal shape engineering. *Ind. Eng. Chem. Res*. **47**, 9812−9833 (2008).

18. Olafson et al. Early onset of kinetic roughening due to a finite step width in hematin crystallization. *Phys. Rev. Lett.* **119**, 198101 (2017).

19. Zhan, G. L. et al. Observing polymerization in 2D dynamic covalent polymers. *Nature* **603**, 835-840 (2022).

20. Kissel, P. et al. A nanoporous two-dimensional polymer by single-crystal-to-single-crystal photopolymerization. *Nat. Chem.* **6**, 774-778 (2014).

21. Pal, A. et al. Molecular mechanism of physical gelation of hydrocarbons by fatty acid amides of natural amino acids. *Tetrahedron* **63**, 7334–7348 (2007).

22. Zhang, Y. B. et al. Single-crystal structure of a covalent organic framework. *J. Am. Chem. Soc.***135**, 16336-16339 (2013).

23. Feng, X. L. & Schlüter, A. D. Towards macroscopic crystalline 2D polymers. *Angew. Chem. Int. Ed.* **57**, 13748–13763 (2018).

24. Ma, T. Q. et al. Observation of interpenetration isomerism in covalent organic frameworks. *J. Am. Chem. Soc.***140**, 6763−6766 (2018).

25. Zhao, W. et al. Using sound to synthesize covalent organic frameworks in water *Nat. Synth.* **1**, 87-95 (2022).

26. Lin, S. et al. Covalent organic frameworks comprising cobalt porphyrins for catalytic CO_2 reduction in water. *Science* 349, 1208-1213 (2015).

27. Horike, S., Shimomura, S. & Kitagawa, S. Soft porous crystals. *Nat. Chem.* **1**, 695-704 (2009).

28. Peng, Y. W. et al. Room temperature batch and continuous flow synthesis of water-stable covalent organic frameworks (COFs). *Chem. Mater.* **28**, 5095–5101 (2016).

Methods

Synthesis procedures of single-crystal COFs

General procedure A: To grow the single-crystal COFs, we dissolved 0.1 mmol amino-acid derivatives (C_8-GlyA, C_{10}-GlyA, C_{12}-GlyA, C_{14}-GlyA, C_{16}-GlyA, C_{18}-GlyA, C_{16}-*L*-AlaA, C_{16}-*L*-PhalaA, C_{16}-*L*-ValA or C_{16}-*L*-*t*LeuA) and 0.1 mmol sodium hydroxide in 8.5 mL of water at 50 °C under ambient conditions. The solution was stirred for 10 minutes to obtain an emulsion of uniform size, then 0.05 mmol (linker **A**/**B**/**C**/**D**/**E**) was added and stirred. Subsequently, a solution of tetrakis(4-aminophenyl)methane (TAM, 9.5 mg, 0.025 mmol) in 0.2 mol L^{-1} acid (PTSA/HCl/HOAc, 1.5 mL) was added, stirred for 5 minutes. After the completion of the reaction, the product was collected by centrifugation and washed three times with water and tetrahydrofuran. Further purification of COFs was carried out by immersing in tetrahydrofuran for 24 hours, dried at ambient temperature for 12 hours and 100 °C for 12 hours to afford single-crystal COFs powder.

Gram-scale production of COF-301, COF-300, SYSU-8, SYSU-9 and COF-320 was performed by parallel increase of the molar amounts of added chemicals and volume of reactors:

C_{16}-GlyA (3.134 g, 10 mmol) and linker **A** (0.831 g, 5 mmol) were explored to gain COF-301 (Yield: 92%, 1.48 g) *under general procedure A*. Recovering rate of C_{16}-GlyA: 93%, 2.91 g.

C_{16}-GlyA (3.134 g, 10 mmol) and linker **B** (0.671 g, 5 mmol) were explored to gain COF-300 (Yield: 95%, 1.37 g) *under general procedure A*. Recovering rate of C_{16}-GlyA: 96%, 3.01 g;

C_{16}-GlyA (3.134 g, 10 mmol) and linker **C** (1.030 g, 5 mmol) were explored to SYSU-8 (Yield: 94%, 1.69 g) *under general procedure A*. Recovering rate of C_{16}-GlyA: 97%, 3.03 g;

C_{16}-GlyA (3.134 g, 10 mmol) and linker **D** (0.676 g, 5 mmol) were explored to gain SYSU-9 (Yield: 93%, 1.35 g) *under general procedure A*. Recovering rate of C_{16}-GlyA: 92%, 2.88 g.

C_{16}-GlyA (3.134 g, 10 mmol) and linker **E** (1.051 g, 5 mmol) were explored to gain COF-320 (Yield: 94%, 1.72 g) *under general procedure A*. Recovering rate of C_{16}-GlyA: 92%, 2.88 g.

Synthesis procedures of 2DCOF-TTA-BTA

To grow the 2D COFs, we dissolved 0.1 mmol C_{16}-*L*-ValA and 0.1 mmol sodium hydroxide in 10 mL of water. Stir at 50 ℃ for 10 minutes to obtain an emulsion of uniform size, then benzene-1,3,5-tricarbaldehyde (BTA, 4.1 mg, 0.025 mmol) was added and stirred. Then a solution of 4,4',4''-(1,3,5-triazine-2,4,6-triyl)trianiline (TTA, 8.85 mg, 0.025 mmol) in 0.2 mol L^{-1} PTSA (1.5 mL) was added, stirred for 5 minutes. After the completion of the reaction, the product was collected by centrifugation and washed three times with water and tetrahydrofuran. Further purification of COFs was carried out by immersing in tetrahydrofuran for 24 hours, dried at ambient temperature for 12 hours and 100 ℃ for 12 hours to afford 2DCOF-TTA-BTA powder. **Gram-scale production:** C_{16}-*L*-ValA (3.556 g, 10 mmol), TTA (885 g, 2.5 mmol) and BTA (410 g, 2.5 mmol) were explored to gain highly crystalline 2DCOF-TTA-BTA powder (Yield: 92%, 1.07 g). Recovering rate of C_{16}-*L*-ValA: 92%, 3.27 g.

Synthesis procedures of single-crystal COF-366

P-toluenesulfonic acid monohydrate (PTSA)was dissolved in water to prepare 2 mol L^{-1} PTSA aqueous solutions. Then 5,10,15,20-Tetrakis (4-aminophenyl)-21H,23H-porphyrin (TAPP) was dissolved in 2 mol L^{-1} PTSA solution to prepare 1 mg mL^{-1} TAPP solution. 2,5-Dihydroxyterephthalaldehyde is dissolved in ethylene glycol solution to prepare 1mg mL^{-1} 2,5-Ph solution. All solutions are sonicated for 30 minutes prior to use.

In a general synthetic procedure 25 mL water was added in a petri dish with a diameter of 56 mm and a height of 16 mm. An ethanol solution of C_{16}-*L*-*t*LeuA (60 μL, 1 mg mL^{-1}) was spread at the air–water interface and left undisturbed for 30 minutes. Solution of TAPP protonated with 2 mol L^{-1} PTSA (200 μL, 0.3 μmol) was added to the petri dish and left undisturbed for 60 minutes. Then, the aqueous solution of aldehyde monomers was slowly injected into the container. Single-crystal COF-366 were obtained after one week. The films were then transferred onto substrates of interest from the air-water surface and cleaned with water and chloroform before characterization.

Data availability

All data supporting the findings of this study are available within the paper and its Supplementary Information files. Additionally, the X-ray crystallographic coordinates for the structures reported in this Article have been deposited at the Cambridge Crystallographic Data Centre (CCDC), under deposition numbers of CCDC 2049342 (C_{16}-*L*-*t*LeuA), CCDC 2209466 (COF-301-S), CCDC 2049378 (SYSU-9-S) and CCDC 2245942 (COF-320).

Additional information

Supplementary information

Correspondence and requests for materials should be addressed to liuw226@mail.sysu.edu.cn; junliang.sun@pku.edu.cn; zhengzhikun@mail.sysu.edu.cn

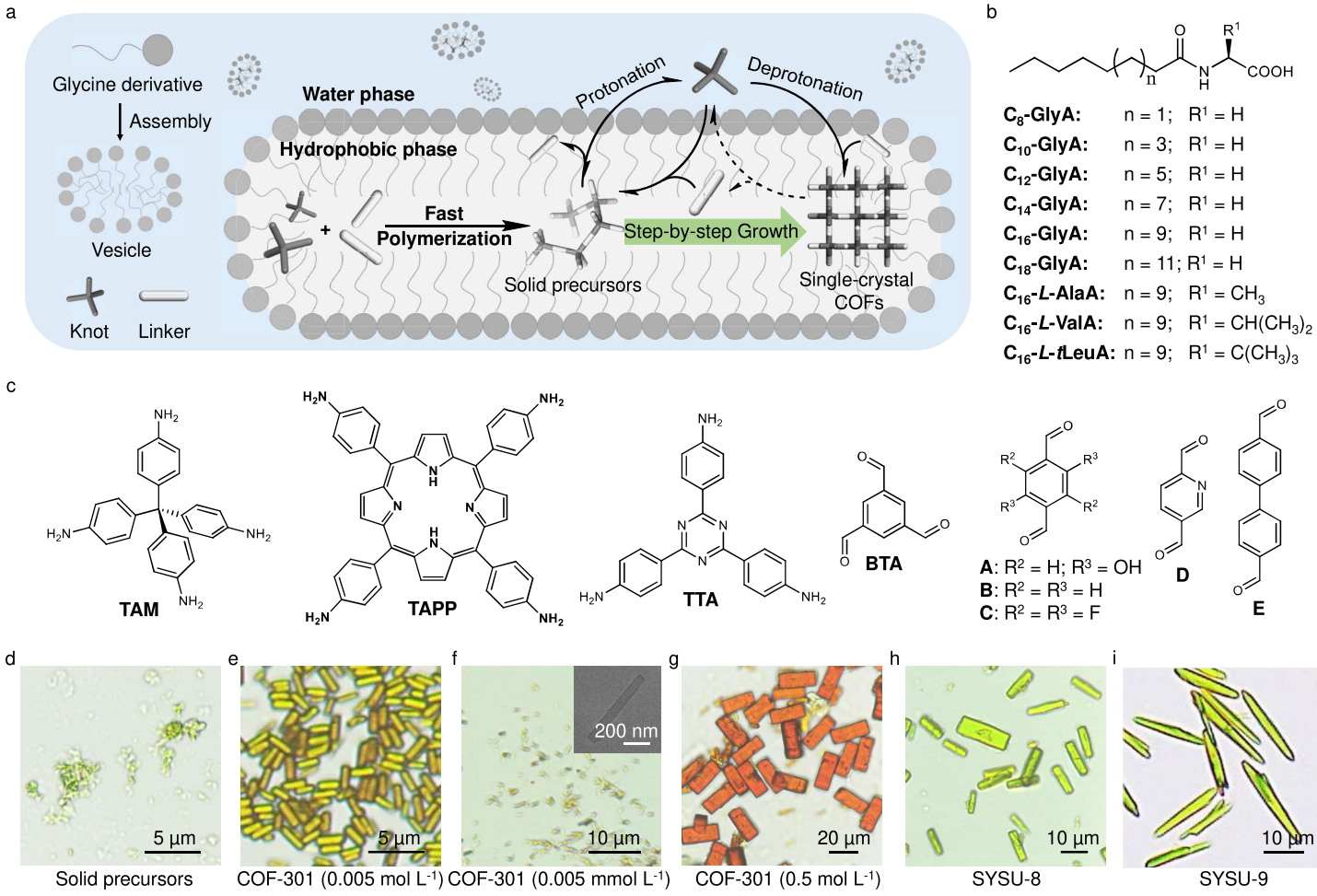
a
Glycine derivative
Assembly
Vesicle
Knot
Linker
Water phase
Hydrophobic phase
Protonation
Deprotonation
Fast
Polymerization
Step-by-step Growth
Solid precursors
Single-crystal
COFs
b
C8-GlyA: n = 1; R1 = H
C10-GlyA: n = 3; R1 = H
C12-GlyA: n = 5; R1 = H
C14-GlyA: n = 7; R1 = H
C16-GlyA: n = 9; R1 = H
C18-GlyA: n = 11; R1 = H
C16-L-AlaA: n = 9; R1 = CH3
C16-L-ValA: n = 9; R1 = CH(CH3)2
C16-L-tLeuA: n = 9; R1 = C(CH3)3
c
TAM
TAPP
TTA
BTA
A: R2 = H; R3 = OH
B: R2 = R3 = H
C: R2 = R3 = F
D
E
d
5 μm
Solid precursors
e
5 μm
COF-301 (0.005 mol L-1)
f
200 nm
10 μm
COF-301 (0.005 mmol L-1)
g
20 μm
COF-301 (0.5 mol L-1)
h
10 μm
SYSU-8
i
10 μm
SYSU-9

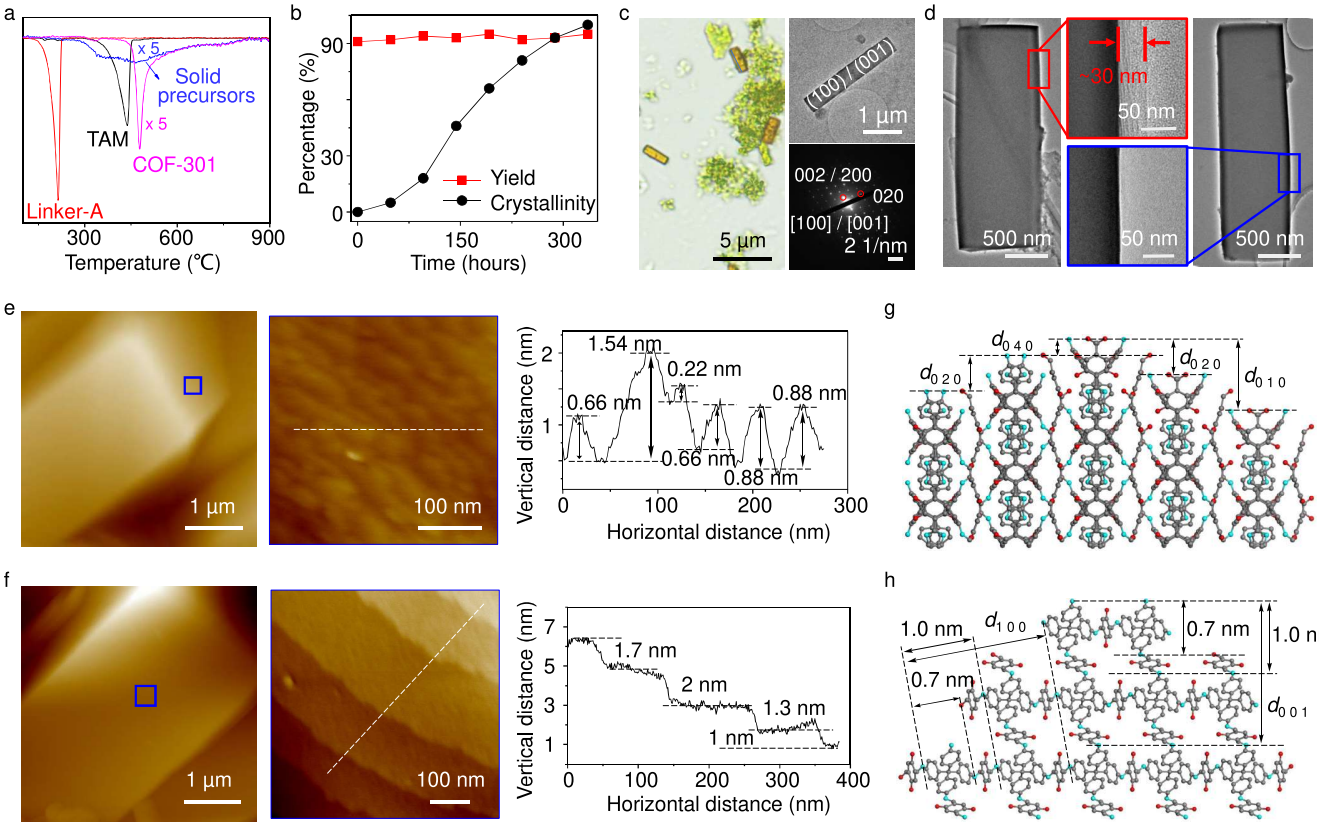
a
x 5
Solid precursors
x 5
TAM
COF-301
Linker-A
300
600
900
Temperature (℃)
b
90
30
0
Percentage (%)
Yield
Crystallinity
0
150
300
Time (hours)
c
5 μm
(100) / (001)
1 μm
002 / 200
020
[100] / [001]
2 1/nm
d
~30 nm
50 nm
500 nm
50 nm
500 nm
e
1 μm
100 nm
Vertical distance (nm)
2
1
1.54 nm
0.22 nm
0.66 nm
0.88 nm
0.66 nm
0.88 nm
0
100
200
300
Horizontal distance (nm)
f
1 μm
100 nm
Vertical distance (nm)
7
5
3
1
1.7 nm
2 nm
1.3 nm
1 nm
0
100
200
300
400
Horizontal distance (nm)
g
d_{040}
d_{020}
d_{020}
d_{010}
h
1.0 nm
d_{100}
0.7 nm
0.7 nm
1.0 nm
d_{001}

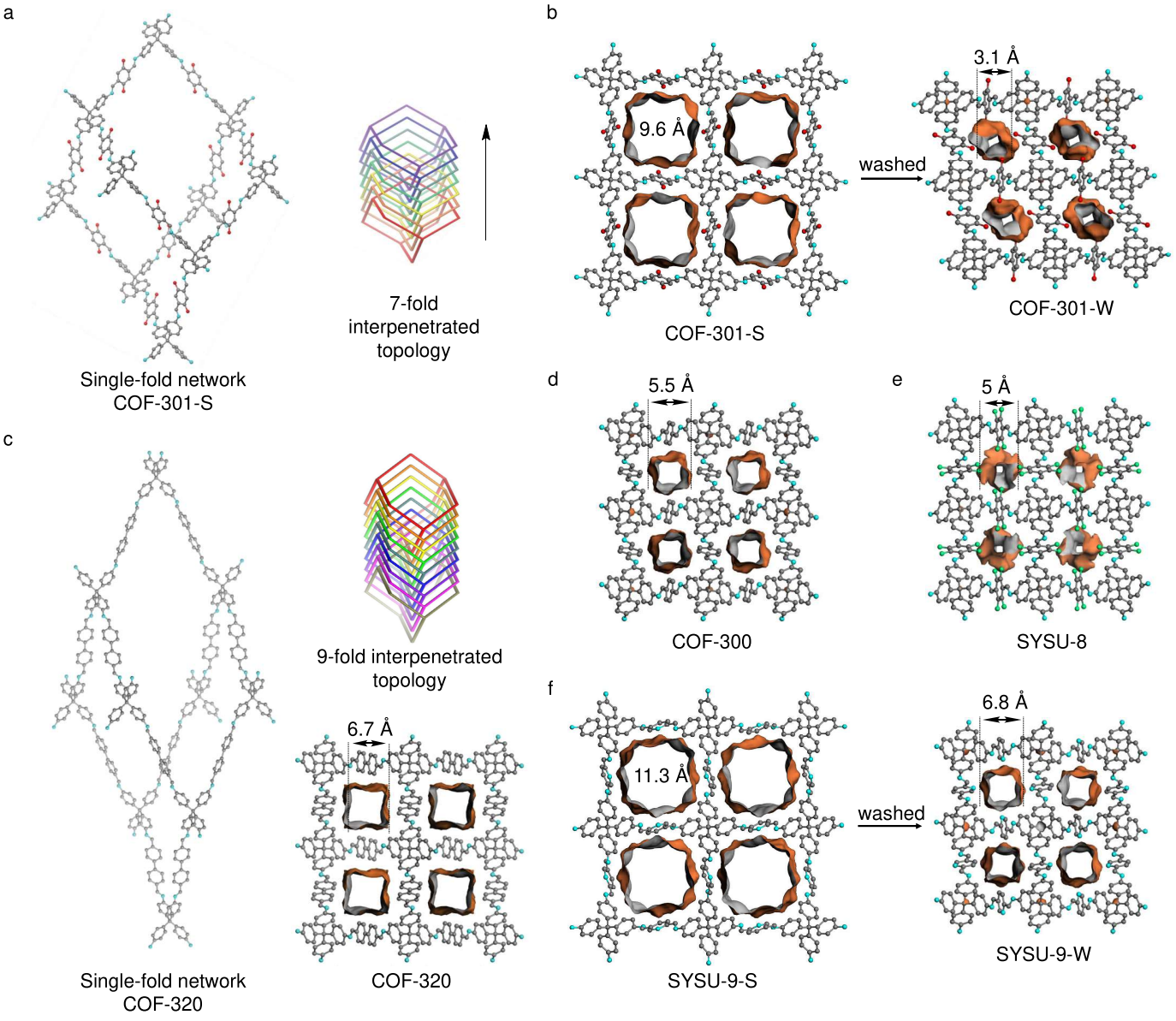
a
Single-fold network
COF-301-S
7-fold
interpenetrated
topology
b
9.6 Å
COF-301-S
washed
3.1 Å
COF-301-W
c
Single-fold network
COF-320
9-fold interpenetrated
topology
6.7 Å
COF-320
d
5.5 Å
COF-300
e
5 Å
SYSU-8
f
11.3 Å
SYSU-9-S
washed
6.8 Å
SYSU-9-W

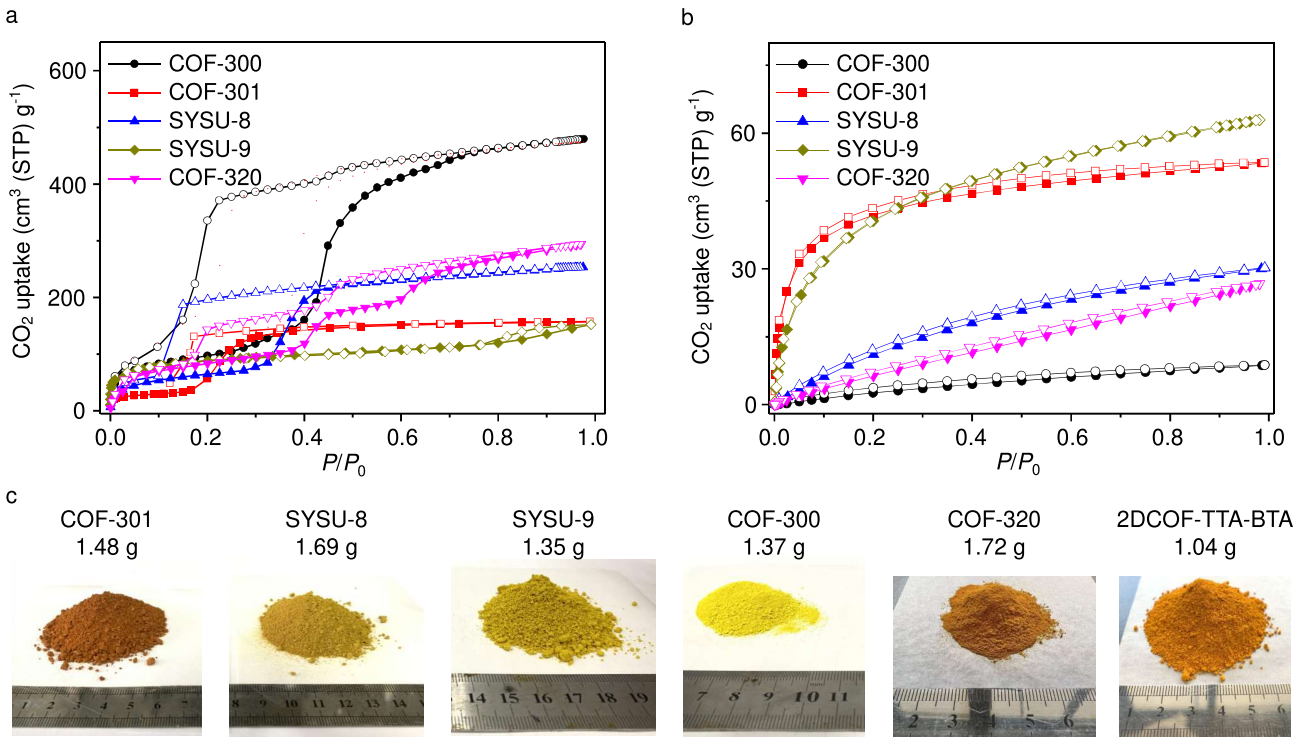
a
b
c
COF-300
COF-301
SYSU-8
SYSU-9
COF-320
CO2 uptake (cm3 (STP) g-1)
P/P0
COF-301
1.48 g
SYSU-8
1.69 g
SYSU-9
1.35 g
COF-300
1.37 g
COF-320
1.72 g
2DCOF-TTA-BTA
1.04 g

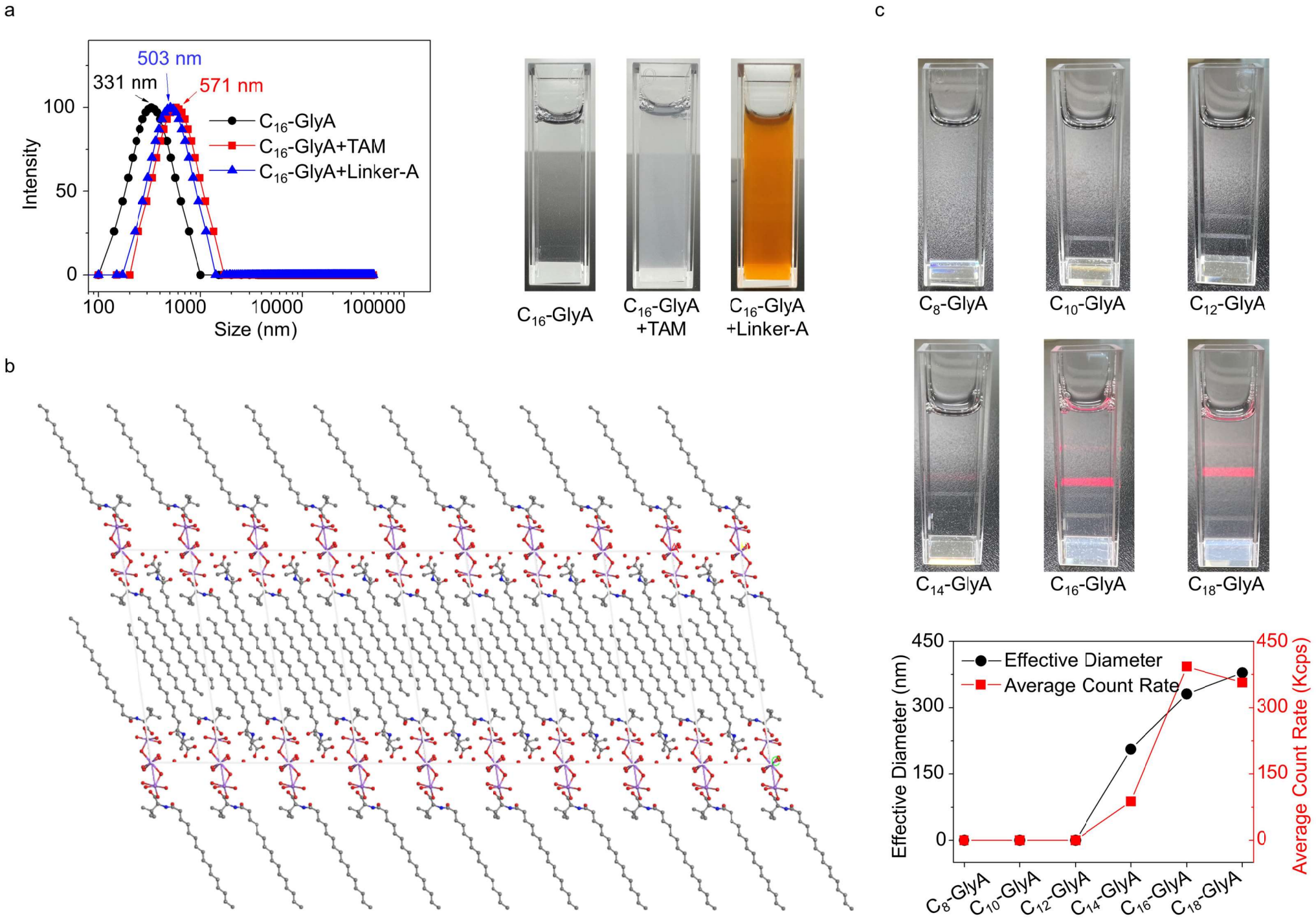
a
503 nm
331 nm
571 nm
100
50
0
Intensity
100
1000
10000
100000
Size (nm)
C16-GlyA
C16-GlyA+TAM
C16-GlyA+Linker-A
C16-GlyA
C16-GlyA +TAM
C16-GlyA +Linker-A
b
c
C8-GlyA
C10-GlyA
C12-GlyA
C14-GlyA
C16-GlyA
C18-GlyA
Effective Diameter
Average Count Rate
Effective Diameter (nm)
Average Count Rate (Kcps)
450
300
150
0
C8-GlyA
C10-GlyA
C12-GlyA
C14-GlyA
C16-GlyA
C18-GlyA

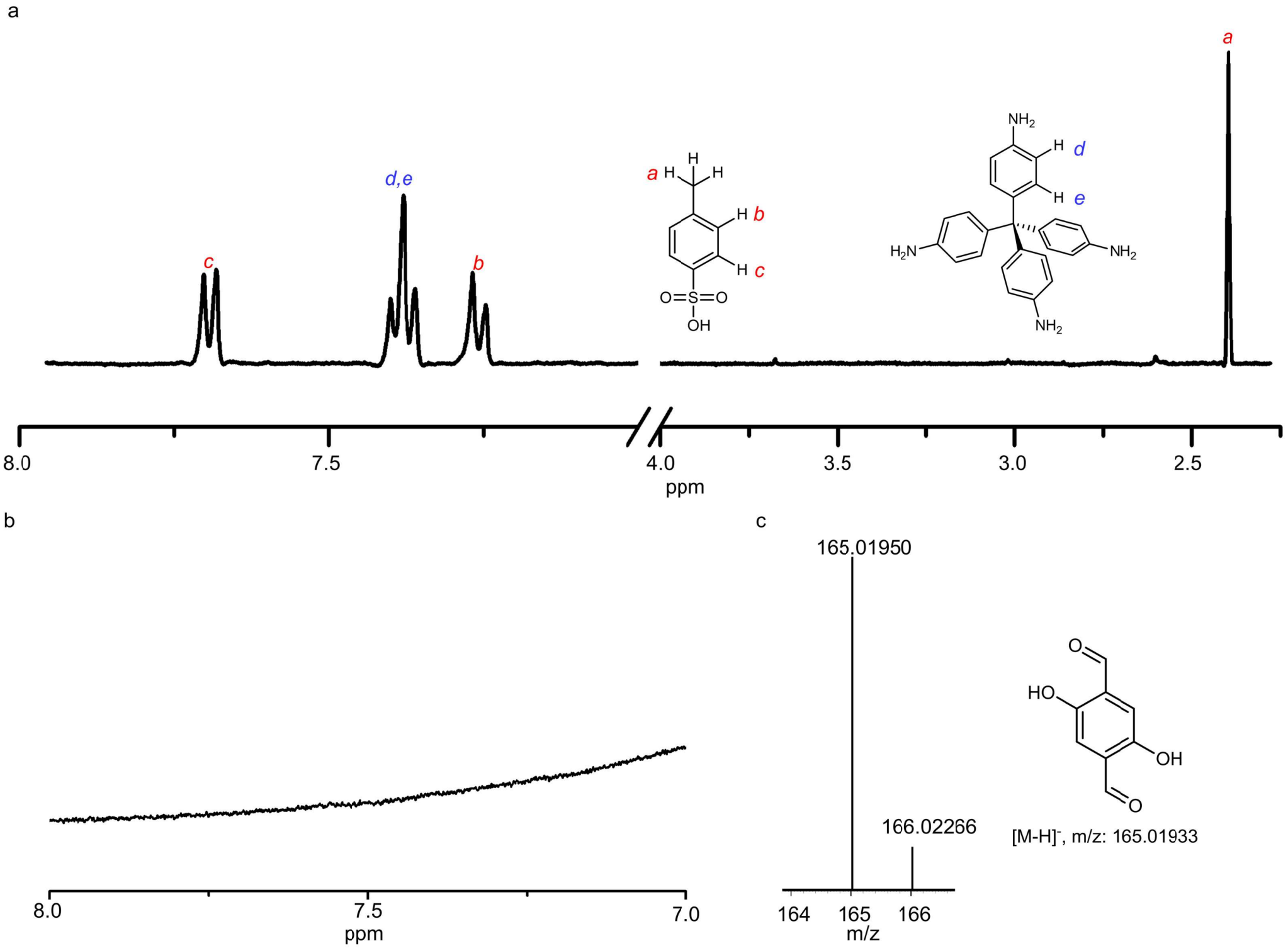
a
a
d,e
c
b
H
H
H
a
H
b
H
c
O=S=O
OH
NH2
H
d
H
e
H2N
NH2
NH2
8.0
7.5
4.0
3.5
3.0
2.5
ppm
b
8.0
7.5
7.0
ppm
c
165.01950
166.02266
164
165
166
m/z
O
HO
OH
O
[M-H]-, m/z: 165.01933

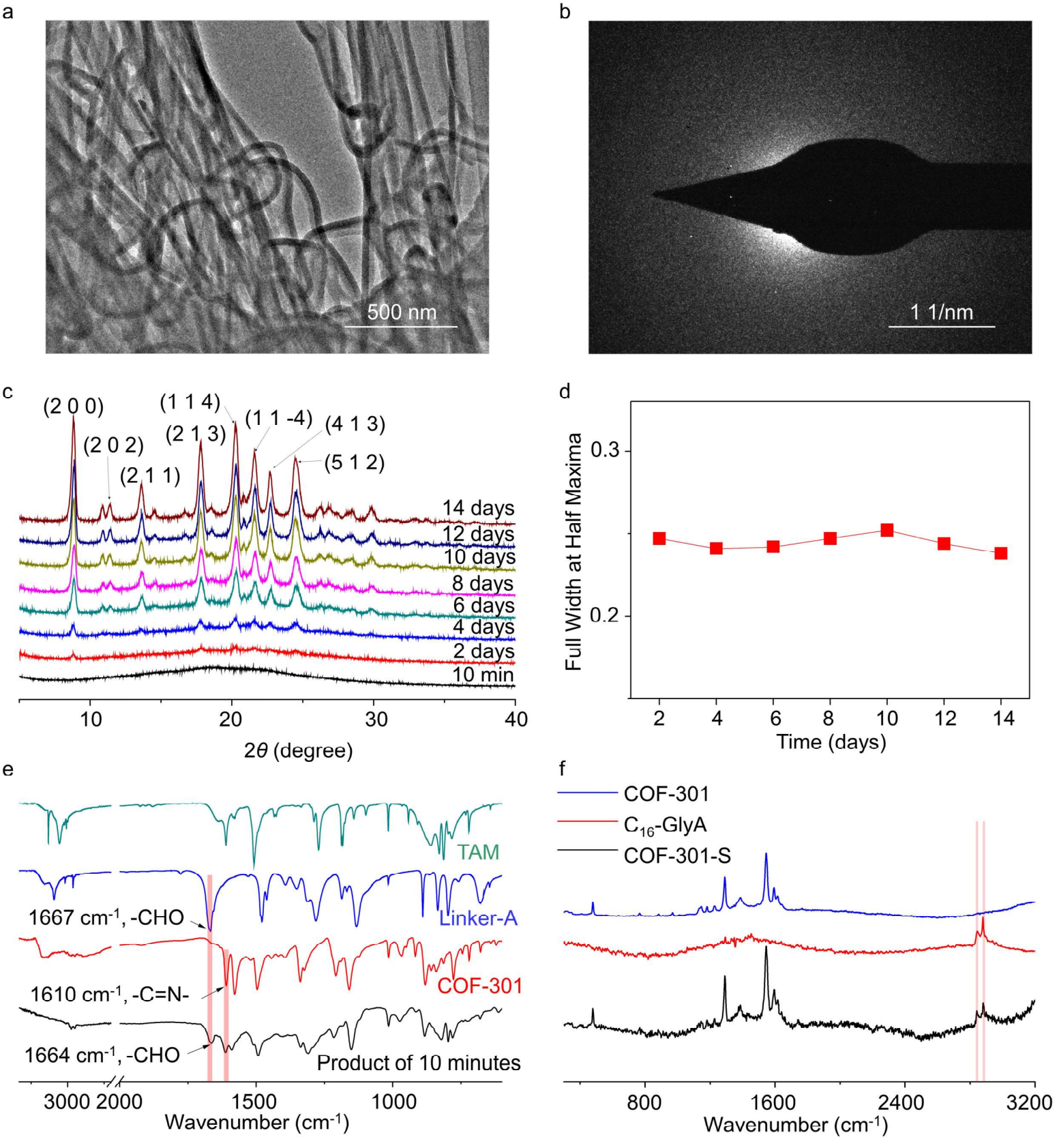
a
500 nm
b
1 1/nm
c
(2 0 0)
(2 0 2)
(2 1 1)
(1 1 4)
(2 1 3)
(1 1 -4)
(4 1 3)
(5 1 2)
14 days
12 days
10 days
8 days
6 days
4 days
2 days
10 min
10
20
30
40
2θ (degree)
d
Full Width at Half Maxima
0.3
0.2
2
4
6
8
10
12
14
Time (days)
e
TAM
Linker-A
COF-301
Product of 10 minutes
1667 cm-1, -CHO
1610 cm-1, -C=N-
1664 cm-1, -CHO
3000 2000
1500
1000
Wavenumber (cm-1)
f
COF-301
C16-GlyA
COF-301-S
800
1600
2400
3200
Wavenumber (cm-1)

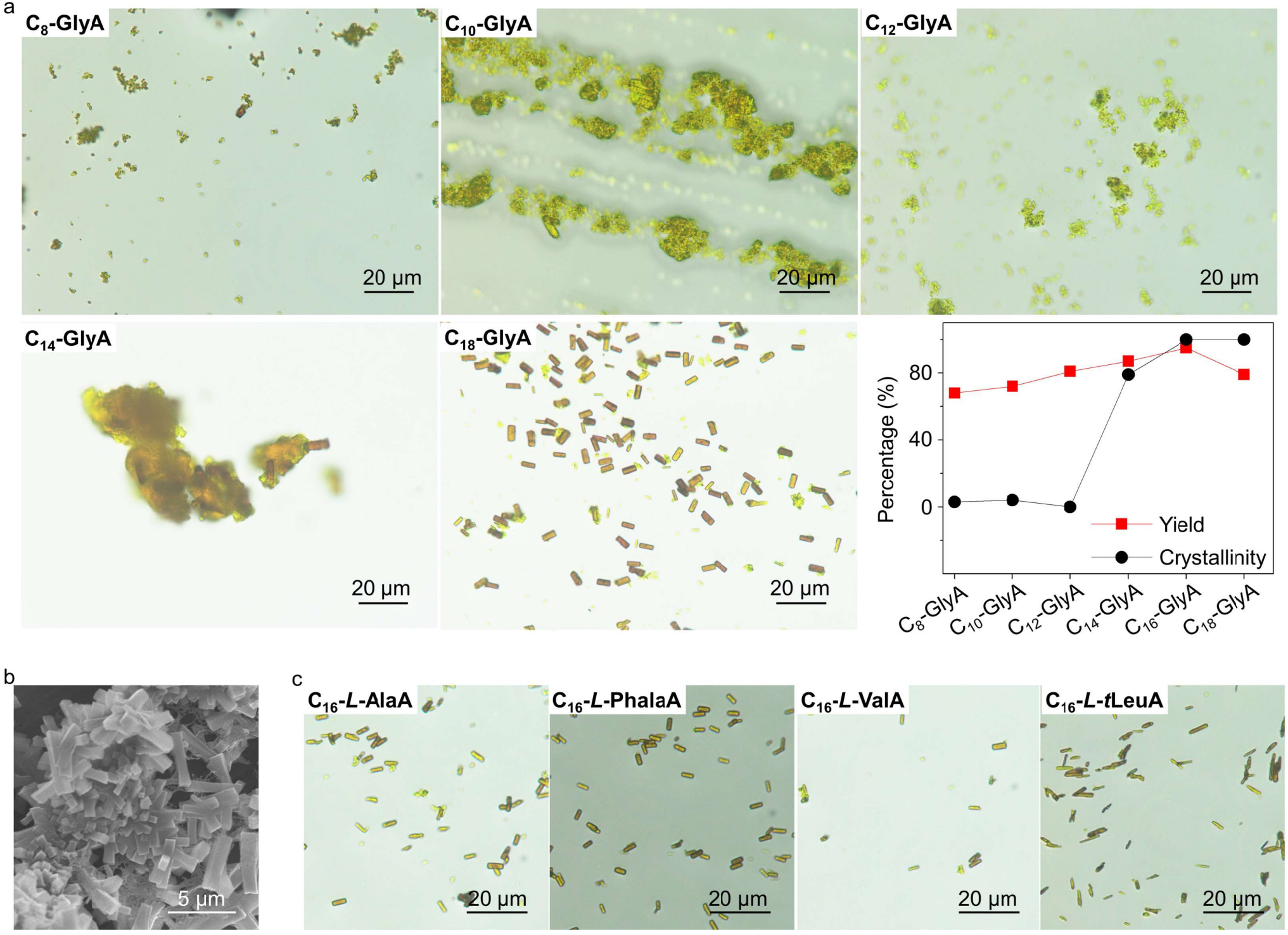
a
C8-GlyA
C10-GlyA
C12-GlyA
C14-GlyA
C18-GlyA
20 μm
Percentage (%)
80
40
0
Yield
Crystallinity
C8-GlyA
C10-GlyA
C12-GlyA
C14-GlyA
C16-GlyA
C18-GlyA
b
5 μm
c
C16-L-AlaA
C16-L-PhalaA
C16-L-ValA
C16-L-tLeuA

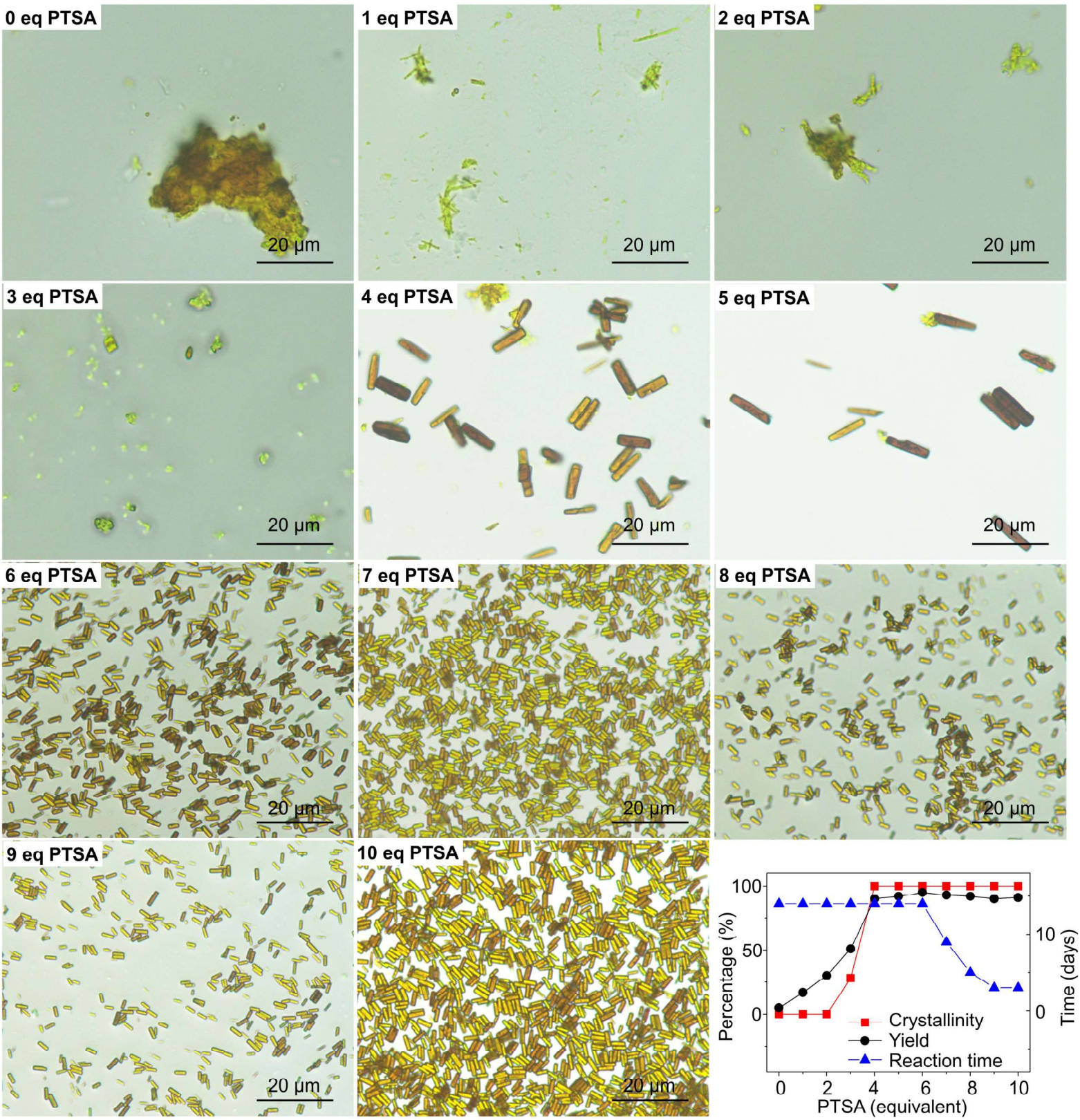
0 eq PTSA
1 eq PTSA
2 eq PTSA
3 eq PTSA
4 eq PTSA
5 eq PTSA
6 eq PTSA
7 eq PTSA
8 eq PTSA
9 eq PTSA
10 eq PTSA
20 μm
Percentage (%)
Time (days)
PTSA (equivalent)
Crystallinity
Yield
Reaction time
0
50
100
2
4
6
8
10

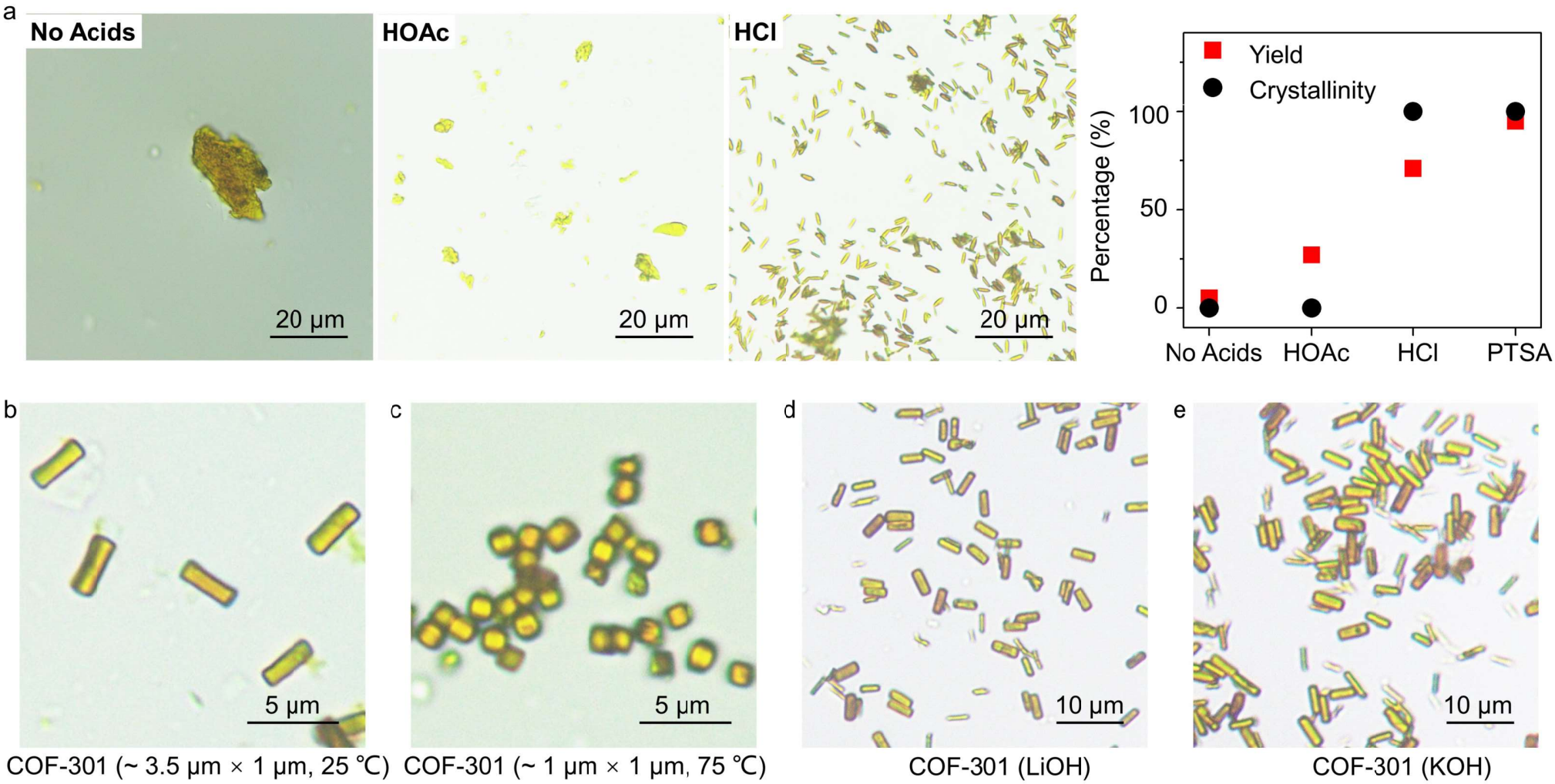
a
No Acids
HOAc
HCl
20 μm
20 μm
20 μm
Yield
Crystallinity
Percentage (%)
100
50
0
No Acids
HOAc
HCl
PTSA
b
c
d
e
5 μm
5 μm
10 μm
10 μm
COF-301 (~ 3.5 μm × 1 μm, 25 ℃)
COF-301 (~ 1 μm × 1 μm, 75 ℃)
COF-301 (LiOH)
COF-301 (KOH)

a

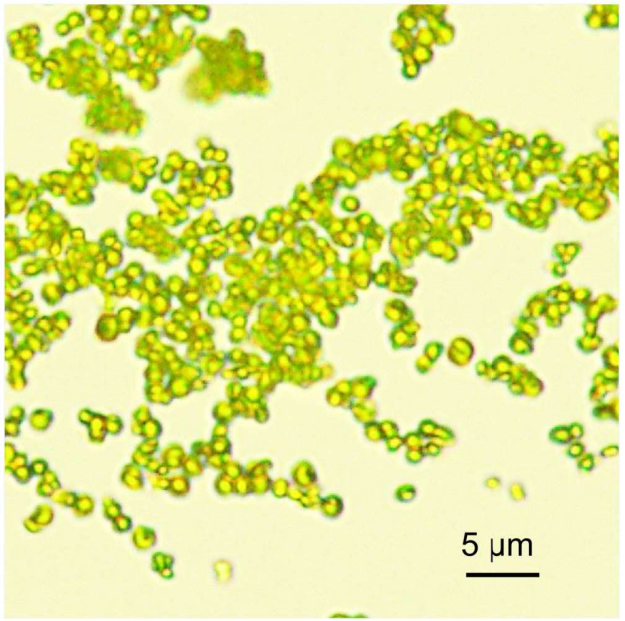

COF-300

b

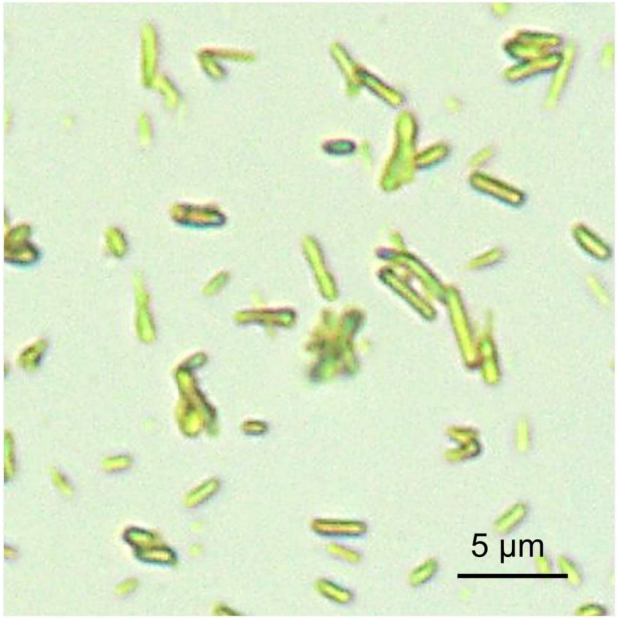

COF-320

c

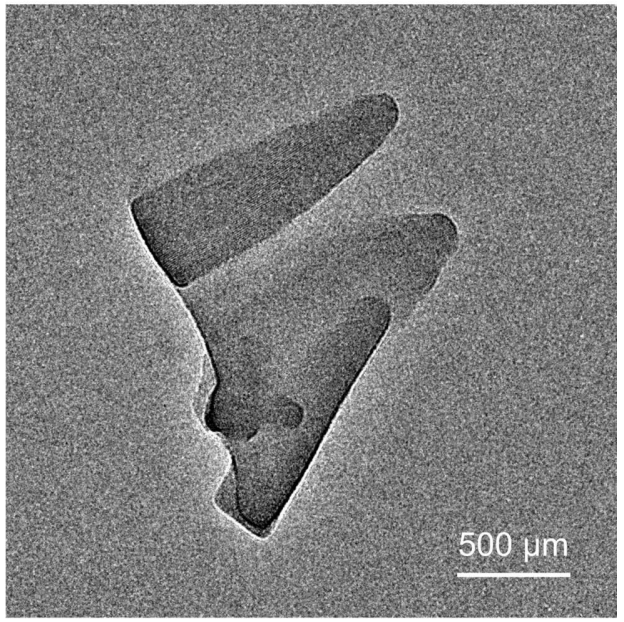

COF-TTA-BTA

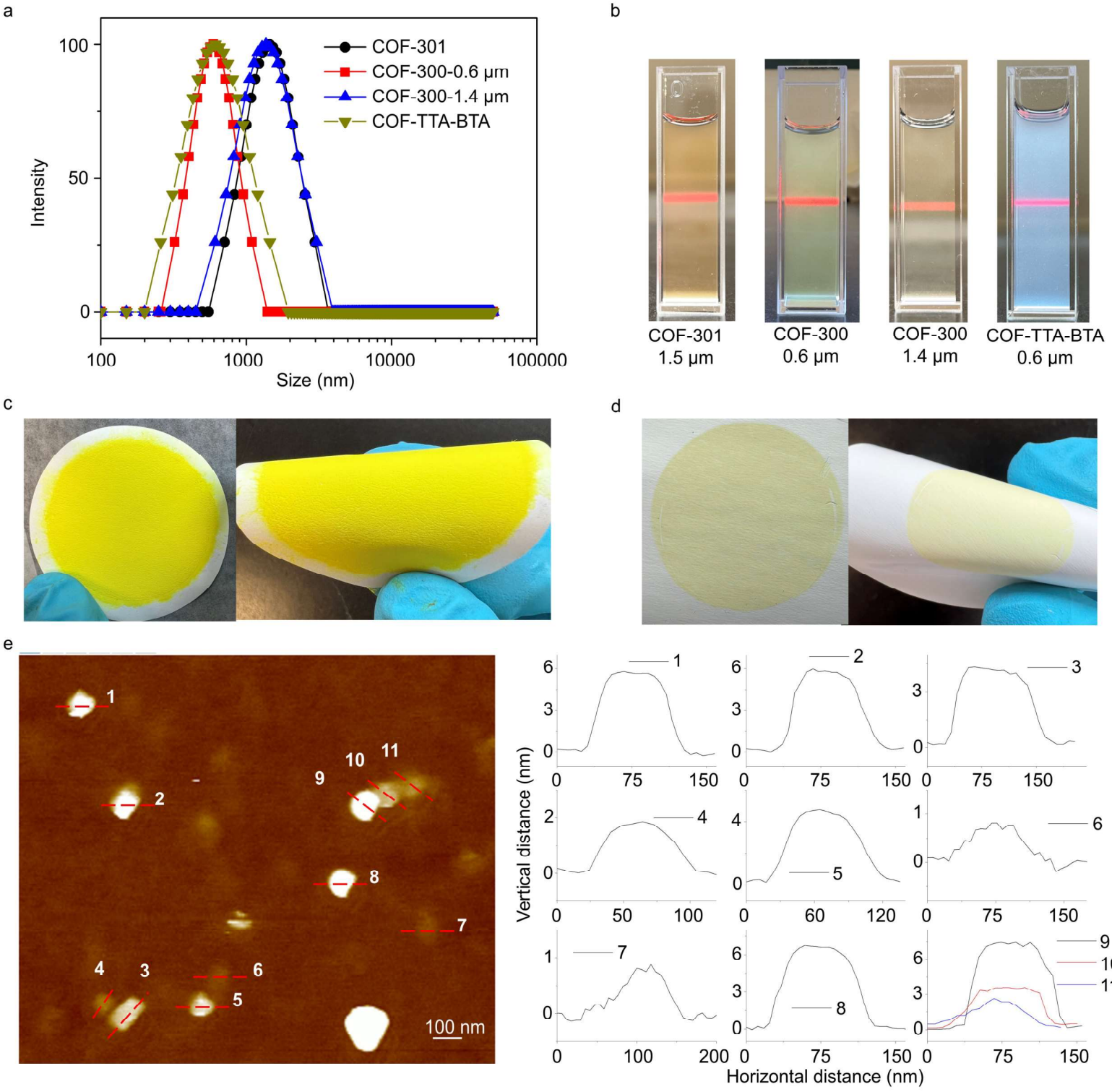
a
100
50
0
Intensity
100
1000
10000
100000
Size (nm)
COF-301
COF-300-0.6 μm
COF-300-1.4 μm
COF-TTA-BTA
b
COF-301
1.5 μm
COF-300
0.6 μm
COF-300
1.4 μm
COF-TTA-BTA
0.6 μm
c
d
e
1
2
3
4
5
6
7
8
9
10
11
100 nm
Vertical distance (nm)
Horizontal distance (nm)
f
50 nm
~1.78 nm

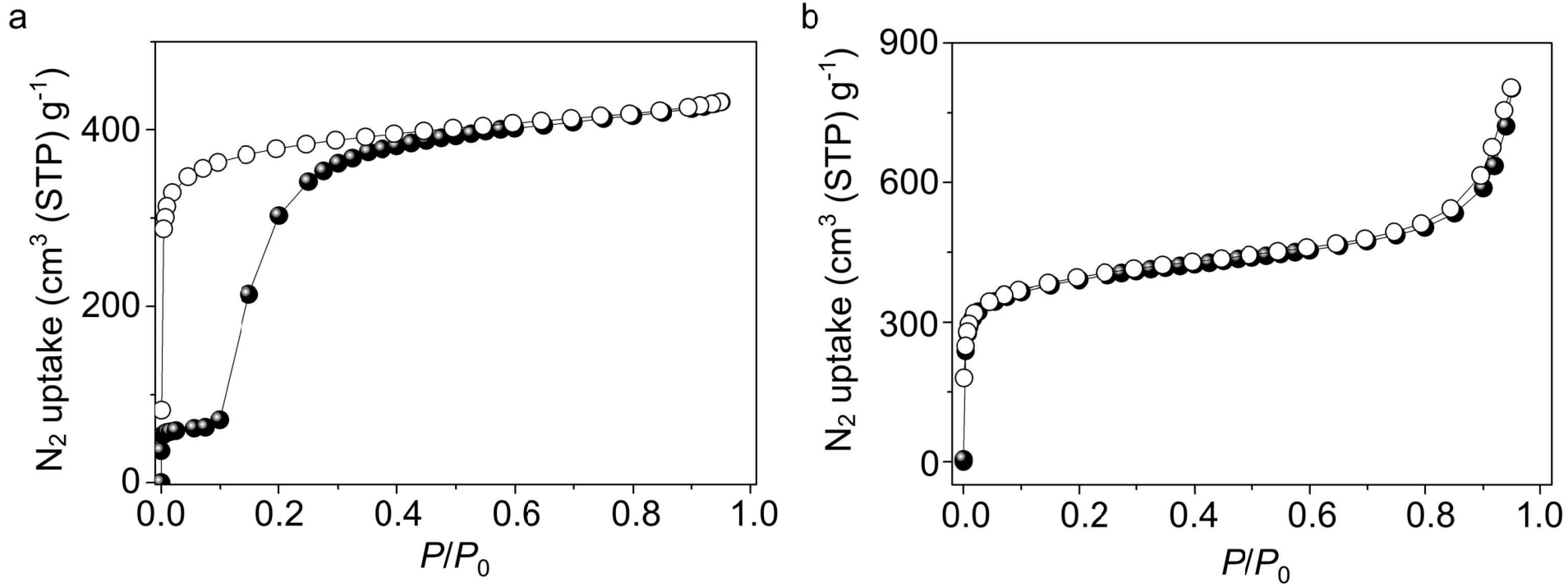
a
b
N2 uptake (cm3 (STP) g-1)
P/P0
0
200
400
300
600
900
0.0
0.2
0.4
0.6
0.8
1.0

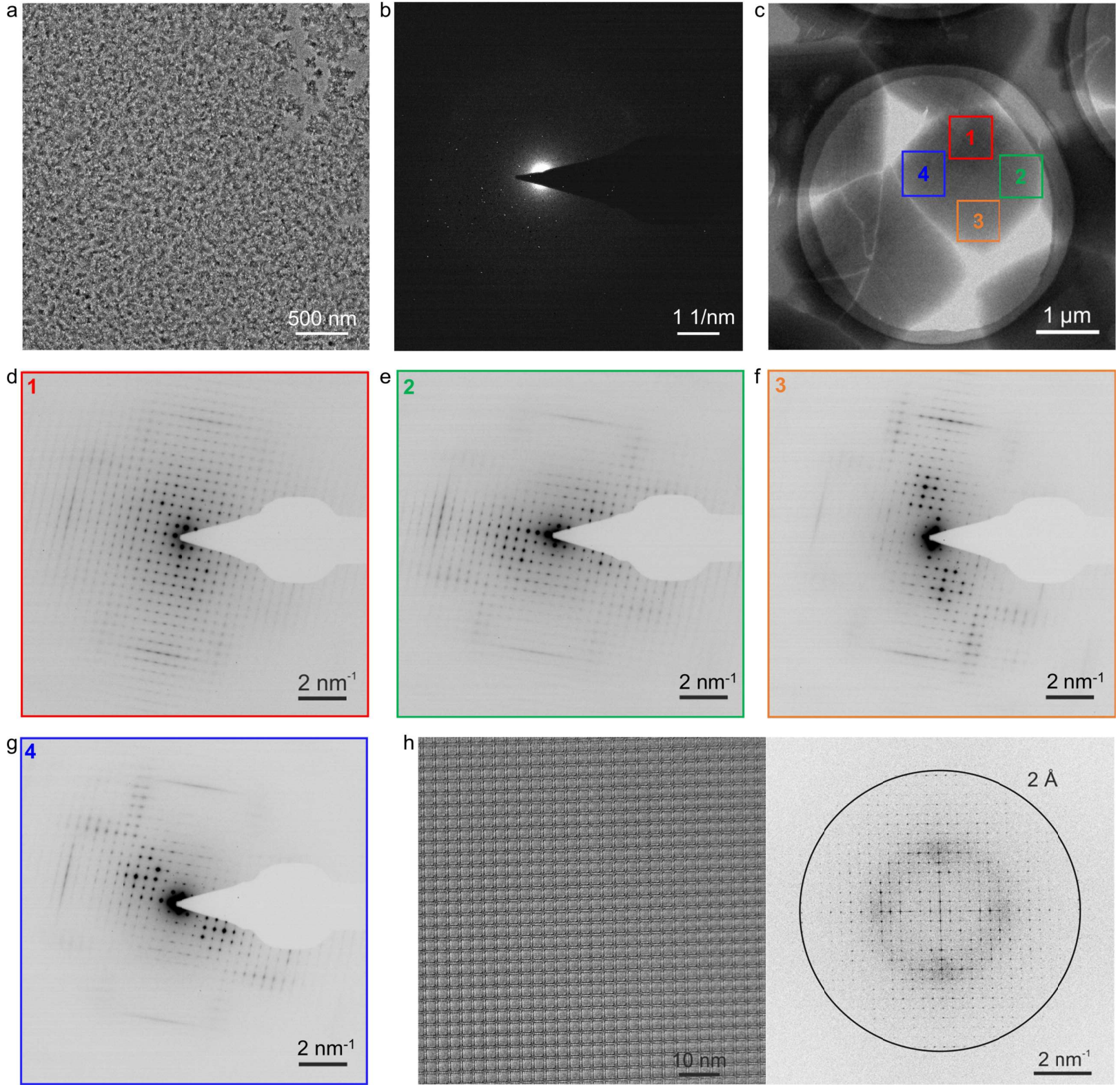
a
500 nm
b
1 1/nm
c
1
2
3
4
1 µm
d
1
2 nm-1
e
2
2 nm-1
f
3
2 nm-1
g
4
2 nm-1
h
10 nm
2 Å
2 nm-1